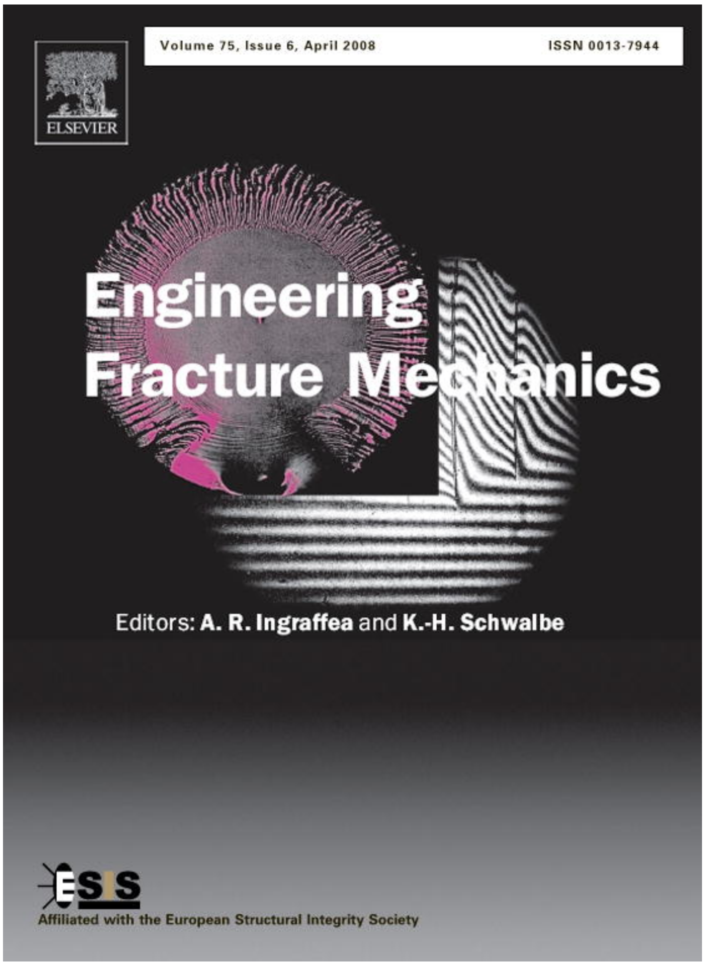
Volume 75, Issue 6, April 2008
ISSN 0013-7944
ELSEVIER
Engineering Fracture Mechanics
Editors: A. R. Ingraffea and K.-H. Schwalbe
ESIS
Affiliated with the European Structural Integrity Society

Available online at www.sciencedirect.com
ScienceDirect
Engineering Fracture Mechanics 75 (2008) 1468–1487
Engineering Fracture Mechanics
www.elsevier.com/locate/engfracmech

Dynamic fracture behavior of an internal interfacial crack between two dissimilar magneto-electro-elastic plates

W.J. Feng [a,*], E. Pan [b]

[a] *Department of Engineering Mechanics, Shijiazhuang Railway Institute, Shijiazhuang 050043, PR China*
[b] *Department of Civil Engineering, The University of Akron, Akron, OH, USA*

Received 22 December 2006; received in revised form 8 May 2007; accepted 2 July 2007
Available online 17 July 2007

Abstract

In this paper, the anti-plane problem for an interfacial crack between two dissimilar magneto-electro-elastic plates subjected to anti-plane mechanical and in-plane magneto-electrical impact loadings is investigated. Four kinds of crack surface conditions are adopted: magneto-electrically impermeable (Case 1), magnetically impermeable and electrically permeable (Case 2), magnetically permeable and electrically impermeable (Case 3), and magneto-electrically permeable (Case 4). The position of the interfacial crack is arbitrary. The Laplace transform and finite Fourier transform techniques are employed to reduce the mixed boundary-value problem to triple trigonometric series equations in the Laplace transform domain. Then the dislocation density functions and proper replacements of the variables are introduced to reduce the series equations to a standard Cauchy singular integral equation of the first kind. The resulting integral equation together with the corresponding single-valued condition is approximated as a system of linear algebra equations, which can easily be solved. Field intensity factors and energy release rates are determined and discussed. The effects of loading combination parameters on dynamic energy release rate are plotted for Cases 1–3. On the other hand, since the magneto-electrically permeable condition is perhaps more physically reasonable for type III crack, the effect of the crack configuration on the dynamic fracture behavior of the crack tips is studied in detail for Case 4. The results could be useful for the design of multilayered magneto-electro-elastic structures and devices.

Keywords: Impact; Magneto-electro-elastic plate; Interfacial crack; Dynamic energy release rate; Singular integral equation; Finite Fourier transform

1. Introduction

Due to their unique magneto-electric coupling effect, composite materials consisting of a piezoelectric phase and a piezomagnetic phase are extensively used as magnetic field probes, electric packaging, acoustic, hydrophones, medical ultrasonic imaging, and sensors and actuators. The mechanics behaviors of these novel materials have drawn significant interest in recent years [1–9].

* Corresponding author. Tel.: +86 311 87936543; fax: +86 311 87935169.
E-mail address: wjfeng999@yahoo.com (W.J. Feng).

0013-7944/$ - see front matter
doi:10.1016/j.engfracmech.2007.07.001

Nomenclature

a, b x-coordinates of crack tips
$B_{Ii}(x,y,t)$, $B_{xi}(x,y,t)$, $B_{yi}(x,y,t)$ magnetic induction components
c half crack length
c_i "extended" shear wave speeds
c^i_{IJKL}, c^i_{44} elastic constants
d width of the plate
$D_{Ii}(x,y,t)$, $D_{xi}(x,y,t)$, $D_{yi}(x,y,t)$ electric displacement components
$\varepsilon^i_{IK}, \varepsilon^i_{11}$ dielectric permittivities
e_x, e_y crack eccentricities away from the horizontal and vertical mid-planes, respectively
e^i_{KIJ}, e^i_{15} piezoelectric constants
$E_{Ki}(x,y,t)$, $E_{xi}(x,y,t)$, $E_{yi}(x,y,t)$ electric field components
$\phi_i(x,y,t)$ electric potentials
f^i_{KIJ}, f^i_{15} piezomagnetic constants
$\gamma_{zyi}(x,y,t)$, $\gamma_{zxi}(x,y,t)$ engineering strain components
g^i_{IK}, g^i_{11} electromagnetic constants
G_a, G_b dynamic energy release rates of crack tips a and b, respectively
h_1, h_2 heights of the plate in the region $y \geqslant 0$ and $y \leqslant 0$, respectively
$H(t)$ heaviside unit step function
$H_{Ki}(x,y,t)$, $H_{yi}(x,y,t)$, $H_{xi}(x,y,t)$ magnetic field components
$\mathbf{K}$ field intensity factor vector
K_T, K_B, K_D stress, magnetic induction and electric displacement intensity factors, respectively
λ_B, λ_D magnetic and electric loading combination parameters, respectively
μ^i_{IK}, μ^i_{11} magnetic permeabilities
p Laplace transform parameter
ρ_i material densities
$\sigma_{IJi}(x,y,t)$, $\sigma_{zxi}(x,y,t)$, $\sigma_{zyi}(x,y,t)$ stress components
$s_{KLi}(x,y,t)$ strain components
t time
$\mathbf{T}_{yi}, \mathbf{T}_{xi}$ "extended" traction vectors
$T^{(j)}_{yi}, T^{(j)}_{xi}$ the jth component of traction vectors
$\mathbf{U}_i$ "extended" displacement vectors
$U^{(j)}_i$ the jth component of displacement vectors
$w_i(x,y,t)$ displacements
x, y, z coordinates
$\psi_i(x,y,t)$ magnetic potentials

On the other hand, when subjected to mechanical, magnetic and electrical loads in service, these magneto-electro-elastic composites can fail prematurely due to defects, such as cracks, holes and inclusions, arising during their manufacturing process. Therefore, it is of great importance to study the fracture behaviors of piezoelectric/piezomagnetic composites with cracks under the magneto-electro-elastic interaction. While a variety of progress has been made on crack problems in magneto-electro-elastic materials [10–14], most studies are for crack problems in homogeneous materials and under static deformation assumption. To date, the analysis of dynamic fracture problems of magneto-electro-elastic materials is still very limited. Du et al. [15] obtained the scattered fields of SH waves by a partially debonded magneto-electro-elastic cylindrical inhomogeneity, and determined the numerical results of crack opening displacement. Feng et al. [16] further investigated both the near- and far-field properties of arc-shaped interfacial cracks. Hou and Leung [17] analyzed the dynamic plane-strain problem of a magneto-electro-elastic hollow cylinder by virtue of the separation of variables, orthogonal expansion technique and the interpolation method. Zhou et al. [18] analyzed the dynamic behavior of two collinear interface cracks in magneto-electro-elastic materials. Feng et al. [19] studied the dynamic fracture behaviors of magneto-electrically impermeable interfacial crack between two dissimilar magneto-electro-elastic materials using the energy density criterion and Fourier integral transform method, where magneto-electrically impermeable crack surface condition was adopted. Hu and Li [20] considered the constant moving crack in an infinite magneto-electro-elastic material. Recently, Hu et al. [21] further studied the moving crack at the interface between two dissimilar magneto-electro-elastic materials, and Feng and Su [22] studied the dynamic fracture behaviors of cracks in a functionally graded magneto-electro-elastic strip, where the Fourier integral transform technique was applied. So far, however, the interfacial crack problems of a magneto-electro-elastic body of finite size, in particular when the problem domain is finite in all directions, have not been addressed.

In this paper, the dynamic anti-plane problem of a bonded magneto-electro-elastic rectangular plate with an interfacial crack is considered. The crack is assumed to be impermeable or permeable for magnetic and electric fields, and the position of the interfacial crack is further assumed to be arbitrary. By virtue of the Laplace transform and finite Fourier transform, the mixed boundary-value problem is first reduced to a singular integral equation in the Laplace transform domain. The resulting singular integral equation is then approximated as a system of linear algebraic equations, which are finally solved. Field intensity factors and dynamic energy release rates (DERRs) in the physical domain are obtained and analyzed. Since for III crack problems (see e.g., [12,13,18,20,21] for magneto-electro-elastic materials and [23] for piezoelectric material), magnetically and/or electrically permeable crack surface conditions are perhaps more reasonable in engineering applications, we emphasize our analysis on Case 4 to show the effects of crack configuration on the DERRs. In the meantime, the effects of the applied magnetic and/or electric excitation on the DERRs for other magneto-electric crack surface assumptions are also simply illustrated. Results presented in this paper should have potential applications to the design of multilayered magneto-electro-elastic structures.

2. Statement of the problem

Consider a Griffith crack of length $b - a$ at arbitrary position of the interface between two bonded magneto-electro-elastic rectangular plates occupying $0 < x < d$, $0 < y < h_1$ and $0 < x < d$, $-h_2 < y < 0$, respectively, as shown in Fig. 1. The magneto-electro-elastic plates are assumed to be transversely isotropic, and be

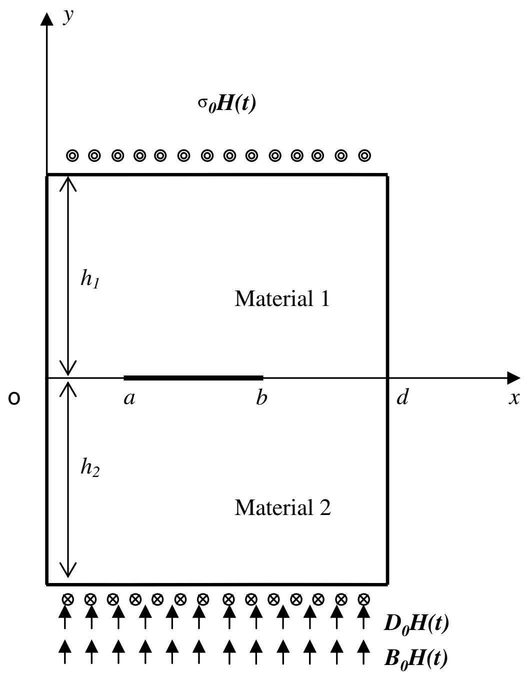

Fig. 1. An interfacial crack between two dissimilar magneto-electro-elastic plates subjected to anti-plane mechanical and in-plane magnetic and electrical impact loadings.

infinitely long in the poling direction, denoted as the z-axis. Within the framework of the theory of linear magneto-electro-elastic solid, the constitutive equations involving stresses σ_{IJ}, strains s_{IJ}, electric displacements D_I, electric fields E_I, magnetic inductions B_I and magnetic fields H_I, are

$$\begin{bmatrix} \sigma_{IJi} \\ D_{Ii} \\ B_{Ii} \end{bmatrix} = \begin{bmatrix} c^i_{IJKL} & -e^i_{KIJ} & -f^i_{KIJ} \\ e^i_{IKL} & \varepsilon^i_{IK} & g^i_{IK} \\ f^i_{IKL} & g^i_{IK} & \mu^i_{IK} \end{bmatrix} \begin{bmatrix} s_{KLi} \\ E_{Ki} \\ H_{Ki} \end{bmatrix}, \quad i = 1,2, \tag{1}$$

where the quantities with the subscript or subscript i (=1, 2), denote the corresponding quantities in the upper and lower plates, respectively; c_{IJKL}, e_{IJK}, f_{IJK} and g_{IK} are the elastic, piezoelectric, piezomagnetic and electromagnetic constants, respectively; ε_{IK} and μ_{IK} are the dielectric permittivities and magnetic permeabilities, respectively. In this paper, only the anti-plane deformation is considered (i.e., anti-plane elastic deformation and in-plane electric and magnetic fields).

When subjected to the anti-plane mechanical and in-plane electric displacement and magnetic induction impact loadings, the constitutive equations in the bonded rectangular plate reduce to

$$\mathbf{T}_{\Lambda i} = \begin{bmatrix} c^i_{44} & -e^i_{15} & -f^i_{15} \\ e^i_{15} & \varepsilon^i_{11} & g^i_{11} \\ f^i_{15} & g^i_{11} & \mu^i_{11} \end{bmatrix} \begin{bmatrix} \gamma_{z\Lambda i} \\ E_{\Lambda i} \\ H_{\Lambda i} \end{bmatrix}, \quad i = 1,2, \quad \Lambda = y, x, \tag{2}$$

where

$$\mathbf{T}_{\Lambda i}(x,y,t) = [\,\sigma_{z\Lambda i}(x,y,t) \quad D_{\Lambda i}(x,y,t) \quad B_{\Lambda i}(x,y,t)\,]^{\mathrm{T}}, \quad i = 1,2, \quad \Lambda = y, x, \tag{3}$$

The strain components $\gamma_{z\Lambda}$ (instead of $2s_{z\Lambda}$ in 1), electric field components E_Λ and magnetic field components H_Λ can be expressed in terms of the out-of-plane displacement w, in-plane electric potential ϕ and magnetic potential ψ by the gradient relations

$$\begin{bmatrix} \gamma_{z\Lambda i} \\ E_{\Lambda i} \\ H_{\Lambda i} \end{bmatrix} = \begin{bmatrix} w_{i,\Lambda} \\ -\phi_{i,\Lambda} \\ -\psi_{i,\Lambda} \end{bmatrix}, \quad i = 1,2, \quad \Lambda = y, x. \tag{4}$$

Neglecting body forces, electric charge density and magnetic current density, it follows that $w(x,y,t)$, $\phi(x,y,t)$ and $\psi(x,y,t)$ satisfy the basic governing partial differential equations for the magneto-electro-elastic body under anti-plane deformation, as

$$\boldsymbol{\Xi}_i \nabla^2 \mathbf{U}_i = [\,\rho_i \partial^2 w_i / \partial t^2 \quad 0 \quad 0\,]^{\mathrm{T}}, \quad i = 1,2, \tag{5}$$

where ∇^2 is the two-dimensional Laplacian operator, ρ_i is the material density, and

$$\boldsymbol{\Xi}_i = \begin{bmatrix} c^i_{44} & e^i_{15} & f^i_{15} \\ e^i_{15} & -\varepsilon^i_{11} & -g^i_{11} \\ f^i_{15} & -g^i_{11} & -\mu^i_{11} \end{bmatrix}, \quad \mathbf{U}_i(x,y,t) = \begin{bmatrix} w_i(x,y,t) \\ \phi_i(x,y,t) \\ \psi_i(x,y,t) \end{bmatrix}, \quad i = 1,2. \tag{6}$$

Introducing

$$\mathbf{U}_i = \boldsymbol{\Omega}_i \mathbf{Z}_i, \quad i = 1,2, \tag{7}$$

where

$$\boldsymbol{\Omega}_i = \begin{bmatrix} 1 & 0 & 0 \\ a_{1i} & b_{1i} & c_{1i} \\ a_{2i} & b_{2i} & c_{2i} \end{bmatrix}, \quad \mathbf{Z}_i(x,y,t) = \begin{bmatrix} w_i(x,y,t) \\ \chi_i(x,y,t) \\ \zeta_i(x,y,t) \end{bmatrix}, \quad i = 1,2, \tag{8}$$

with a_{1i}, b_{1i}, c_{1i} (referring to Appendix A) being known constants, the constitutive Eq. (2) and governing Eq. (5) can be respectively expressed as

$$\mathbf{T}_{\Lambda i} = \mathbf{M}_i \frac{\partial \mathbf{Z}_i}{\partial \Lambda}, \quad i = 1, 2, \quad \Lambda = y, x, \tag{9}$$

$$\nabla^2 \mathbf{Z}_i = [\, c_i^{-2} \partial^2 w_i / \partial t^2 \quad 0 \quad 0 \,]^{\mathrm{T}}, \quad i = 1, 2, \tag{10}$$

where

$$\mathbf{M}_i = \begin{bmatrix} m_{1i} & m_{2i} & m_{3i} \\ 0 & 1 & 0 \\ 0 & 0 & 1 \end{bmatrix}, \quad i = 1, 2, \quad \Lambda = y, x, \tag{11}$$

with m_{1i}, m_{2i} and m_{3i} again referring to Appendix A, and $c_i = \sqrt{m_{1i}/\rho_i}(i = 1, 2)$ is the "extended" shear wave speed.

For the present crack problem, four kinds of ideal magneto-electric boundary condition are assumed by extending the conception of the electrically impermeable and permeable crack embedded in a piezoelectric material [24]. They are, respectively, (i) magneto-electrically impermeable, (ii) magnetically impermeable and electrically permeable, (iii) magnetically permeable and electrically impermeable, and (iv) magneto-electrically permeable. Thus, the crack surface conditions can be described as

Case 1:

$$T_{yi}^{(j)}(x, 0, t) = 0, \quad j = 1, 2, 3, \quad i = 1, 2, \quad a < x < b, \tag{12}$$

Case 2:

$$T_{yi}^{(j)}(x, 0, t) = 0, \quad j = 1, 3, \quad i = 1, 2, \quad a < x < b, \tag{13}$$

$$U_1^{(2)}(x, 0, t) = U_2^{(2)}(x, 0, t), \quad a < x < b, \tag{14}$$

Case 3:

$$T_{yi}^{(j)}(x, 0, t) = 0, \quad j = 1, 2, \quad i = 1, 2, \quad a < x < b, \tag{15}$$

$$U_1^{(3)}(x, 0, t) = U_2^{(3)}(x, 0, t), \quad a < x < b, \tag{16}$$

Case 4:

$$T_{yi}^{(1)}(x, 0, t) = 0, \quad i = 1, 2, \quad a < x < b, \tag{17}$$

$$U_1^{(j)}(x, 0, t) = U_2^{(j)}(x, 0, t), \quad j = 2, 3, \quad a < x < b, \tag{18}$$

where the quantities with superscript (j) (j = 1, 2, 3) represent the elements of the jth column in the corresponding vector. Moreover, due to the presence of the interface bonding regions, the elastic displacements, electric potentials, magnetic potentials, stresses, electric displacements and magnetic inductions should be continuous across the interface, which can be written as

$$\mathbf{U}_1(x, 0, t) = \mathbf{U}_2(x, 0, t), \quad \mathbf{T}_{y1}(x, 0, t) = \mathbf{T}_{y2}(x, 0, t), \quad x \notin (a, b). \tag{19}$$

In addition, there exist eight possible boundary conditions for the applied magneto-electro-mechanical uniform impact loadings at the edges of the bonded plate. For simplicity, only one of them is considered, i.e.,

$$\mathbf{T}_{y1}(x, h_1, t) = \mathbf{T}_{y2}(x, -h_2, t) = \boldsymbol{\tau}_0 H(t), \quad 0 < x < d, \tag{20}$$

$$\mathbf{T}_{x1}(0, y, t) = \mathbf{T}_{x1}(d, y, t) = 0, \quad 0 < y < h_1, \tag{21}$$

$$\mathbf{T}_{x2}(0, y, t) = \mathbf{T}_{x2}(d, y, t) = 0, \quad -h_2 < y < 0, \tag{22}$$

where $H(t)$ is the unit step function, and $\boldsymbol{\tau}_0 = [\, \sigma_0 \quad D_0 \quad B_0 \,]^{\mathrm{T}}$ is the given loading coefficient. Eqs. (20)–(22) indicate that the bonded plate is initially at rest. At time $t = 0$, the anti-plane shear loading σ_0, electric displacement D_0 and magnetic induction B_0 are applied suddenly to both the upper and lower surfaces and maintained constants thereafter. Moreover, both the left- and right-hand sides of the plate are assumed to be traction free, with also the normal electric displacement and magnetic induction being zero.

3. Solution and analysis of magneto-electrically impermeable interfacial cracks (Case 1)

3.1. Derivation and solution of singular integral equation

We define a Laplace transform pair as follows:

$$f^*(p) = \int_0^\infty f(t)\mathrm{e}^{-pt}\,\mathrm{d}t, \quad f(t) = \frac{1}{2\pi i}\int_{\mathrm{Br}} f^*(p)\mathrm{e}^{pt}\,\mathrm{d}p, \tag{23}$$

in which Br stands for the Bromwich path of integration, p denotes the Laplace parameter. Thus it follows from Eq. (10) that in Laplace transform domain,

$$\nabla^2\mathbf{Z}_i^* - \begin{bmatrix} p^2c_i^{-2}w_i^* & 0 & 0\end{bmatrix}^{\mathrm{T}} = 0, \quad i = 1, 2. \tag{24}$$

In previous studies on cracks in magneto-electro-elastic materials, the Fourier transform method is frequently used [13,14,16,18,19]. However, for the present study we propose the Fourier series approach or the finite Fourier transform technique, since it can avoid some tedious manipulations in the derivation as compared to the usual Fourier integral transform method. Based on the above method, it can be easily shown that an appropriate solution satisfying Eq. (24) can be written in terms of the following Fourier series:

$$\begin{aligned}\mathbf{Z}_i^*(x,y,p) = {}& \sum_{n=1}^{\infty}\{\mathrm{diag}\left[\mathrm{e}^{-\lambda_{ni}y}, \mathrm{e}^{-\beta_n y}, \mathrm{e}^{-\beta_n y}\right]\mathbf{A}_{ni}(p) + \mathrm{diag}\left[\mathrm{e}^{\lambda_{ni}y}, \mathrm{e}^{\beta_n y}, \mathrm{e}^{\beta_n y}\right]\mathbf{B}_{ni}(p)\}\cos(\beta_n x) \\ & + \frac{1}{p}\mathbf{M}_i^{-1}\mathbf{C}_{0i}y + \mathbf{Z}_{0i}^*(p), \quad i = 1, 2,\end{aligned} \tag{25}$$

where

$$\lambda_{ni}(p) = \sqrt{\beta_n^2 + p^2 v_i^{-2}}, \quad \beta_n = n\pi/d, \tag{26}$$

$\mathbf{A}_{ni}$, $\mathbf{B}_{ni}$ ($n = 1, 2, \ldots$), $\mathbf{C}_{0i}$ and $\mathbf{Z}_{0i}^*$ are unknown vectors to be determined from the appropriate boundary conditions, and $\mathbf{M}_i^{-1}$ is introduced in Eq. (25) purely for convenience.

Once $\mathbf{Z}_i^*(x,y,p)$ are determined from the given boundary conditions, it is straightforward to obtain the series expressions for the components of the anti-plane stresses, in-plane electric displacements and magnetic inductions. They are, respectively,

$$\mathbf{T}_{yi}^*(x,y,p) = -\mathbf{M}_i\sum_{n=1}^{\infty}\left\{\mathrm{diag}\left[\lambda_{ni}\mathrm{e}^{-\lambda_{ni}y}, \beta_n\mathrm{e}^{-\beta_n y}, \beta_n\mathrm{e}^{-\beta_n y}\right]\mathbf{A}_{ni} - \mathrm{diag}\left[\lambda_{ni}\mathrm{e}^{\lambda_{ni}y}, \beta_n\mathrm{e}^{\beta_n y}, \beta_n\mathrm{e}^{\beta_n y}\right]\mathbf{B}_{ni}\right\}\cos(\beta_n x) + \frac{1}{p}\mathbf{C}_{0i}, \tag{27}$$

$$\mathbf{T}_{xi}^*(x,y,p) = -\mathbf{M}_i\sum_{n=1}^{\infty}\left\{\mathrm{diag}\left[\mathrm{e}^{-\lambda_{ni}y}, \mathrm{e}^{-\beta_n y}, \mathrm{e}^{-\beta_n y}\right]\mathbf{A}_{ni} + \mathrm{diag}\left[\mathrm{e}^{\lambda_{ni}y}, \mathrm{e}^{\beta_n y}, \mathrm{e}^{\beta_n y}\right]\mathbf{B}_{ni}\right\}\beta_n\sin(\beta_n x), \tag{28}$$

In what follows, we shall look for these unknown vectors. Firstly, by a simple manipulation, $\mathbf{C}_{0i}$ can be determined from the boundary conditions in the Laplace domain corresponding to Eq. (20) as follows:

$$\mathbf{C}_{0i} = \boldsymbol{\tau}_0. \tag{29}$$

What remains is to determine a singular field disturbed by the interfacial crack between the two dissimilar magneto-electro-elastic plates. In the following, we do not directly solve $\mathbf{A}_{ni}(p)$, $\mathbf{B}_{ni}(p)$ $\quad(n = 1, 2, \ldots)$. Instead, by eliminating them through given boundary conditions, a singular integral equation is obtained. More specifically, making use of the continuity conditions of the stress, electric displacement and magnetic induction at

$y = 0$, and the boundary conditions on the top and bottom surfaces of the rectangular magneto-electro-elastic plate, we obtain, in the Laplace domain,

$$\mathbf{M}_1 \operatorname{diag}[\lambda_{n1}, \beta_n, \beta_n](\mathbf{A}_{n1} - \mathbf{B}_{n1}) = \mathbf{M}_2 \operatorname{diag}[\lambda_{n2}, \beta_n, \beta_n](\mathbf{A}_{n2} - \mathbf{B}_{n2}), \tag{30}$$

$$\operatorname{diag}\left[e^{-\lambda_{n1}h_1}, e^{-\beta_n h_1}, e^{-\beta_n h_1}\right]\mathbf{A}_{n1} - \operatorname{diag}\left[e^{\lambda_{n1}h_1}, e^{\beta_n h_1}, e^{\beta_n h_1}\right]\mathbf{B}_{n1} = 0, \tag{31}$$

$$\operatorname{diag}\left[e^{\lambda_{n2}h_2}, e^{\beta_n h_2}, e^{\beta_n h_2}\right]\mathbf{A}_{n2} - \operatorname{diag}\left[e^{-\lambda_{n2}h_2}, e^{-\beta_n h_2}, e^{-\beta_n h_2}\right]\mathbf{B}_{n2} = 0, \tag{32}$$

for $n = 1, 2, \ldots$. The resulting three algebraic equations for $\mathbf{A}_{n1}$, $\mathbf{A}_{n2}$, $\mathbf{B}_{n1}$ and $\mathbf{B}_{n2}$, are solvable up to three unknowns. Hence, by choosing $\mathbf{B}_{n2}$ as an unknown, we obtain

$$\mathbf{A}_{n1} = \operatorname{diag}\left[e^{2\lambda_{n1}h_1}, e^{2\beta_n h_1}, e^{2\beta_n h_1}\right]\mathbf{L}_n(p)\mathbf{B}_{n2}, \tag{33}$$

$$\mathbf{A}_{n2} = \operatorname{diag}\left[e^{-2\lambda_{n2}h_2}, e^{-2\beta_n h_2}, e^{-2\beta_n h_2}\right]\mathbf{B}_{n2}, \tag{34}$$

$$\mathbf{B}_{n1} = \mathbf{L}_n(p)\mathbf{B}_{n2}, \tag{35}$$

where $\mathbf{L}_n(p)$ is a 3×3 matrix, with its elements being given in Appendix B.

We now define the jumps of the elastic displacement, electric potential and magnetic potential across the crack faces as follows

$$\Delta\mathbf{U}^*(x, 0, p) = \mathbf{U}_1^*(x, 0, p) - \mathbf{U}_2^*(x, 0, p). \tag{36}$$

From Eqs. (7), (25) and (33)–(35), we can easily obtain

$$\Delta\mathbf{U}^*(x, 0, p) = \sum_{n=1}^{\infty}\{\mathbf{\Omega}_1(\mathbf{A}_{n1} + \mathbf{B}_{n1}) - \mathbf{\Omega}_2(\mathbf{A}_{n2} + \mathbf{B}_{n2})\}\cos(\beta_n x) + \mathbf{U}_0^*(p), \tag{37}$$

where

$$\mathbf{U}_0^* = \mathbf{\Omega}_1\mathbf{Z}_{01}^* - \mathbf{\Omega}_2\mathbf{Z}_{02}^*. \tag{38}$$

Substituting Eqs. (33)–(35) into Eq. (37), we can further obtain

$$\Delta\mathbf{U}^*(x, 0, p) = 2\sum_{n=1}^{\infty}\mathbf{C}_n\cos(\beta_n x) + \mathbf{U}_0^*. \tag{39}$$

where

$$\mathbf{C}_n = \frac{1}{2}\mathbf{\Delta}_n\mathbf{B}_{n2}, n = 1, 2, \ldots, \tag{40}$$

with

$$\mathbf{\Delta}_n(p) = \mathbf{\Omega}_1 \operatorname{diag}[\coth(\lambda_{n1}h_1), \coth(\beta_n h_1), \coth(\beta_n h_1)]\mathbf{\Pi}_n(p) - \mathbf{\Omega}_2 \operatorname{diag}\left[e^{-2\lambda_{n2}h_2} + 1, e^{-2\beta_n h_2} + 1, e^{-2\beta_n h_2} + 1\right], \tag{41}$$

and $\mathbf{\Pi}_n(p)$ being given in Appendix B.

From Eqs. (27), (33)–(35) and (40), we arrive at

$$\mathbf{T}_{y2}^*(x, 0, p) = -2\mathbf{M}_2\sum_{n=1}^{\infty}\mathbf{Q}_n\mathbf{C}_n\cos(\beta_n x) + \frac{1}{p}\boldsymbol{\tau}_0, \tag{42}$$

where

$$\mathbf{Q}_n = \operatorname{diag}\left[\lambda_{n2}\left(e^{-2\lambda_{n2}h_2} - 1\right), \beta_n\left(e^{-2\beta_n h_2} - 1\right), \beta_n\left(e^{-2\beta_n h_2} - 1\right)\right]\mathbf{\Delta}_n^{-1}. \tag{43}$$

Applying Eq. (12) and the first of Eq. (19) yields, from Eqs. (42) and (39),

$$-2\mathbf{M}_2\sum_{n=1}^{\infty}\mathbf{Q}_n\mathbf{C}_n\cos(\beta_n x)+\frac{1}{p}\mathbf{C}_0=0,\quad a<x<b, \tag{44}$$

$$2\sum_{n=1}^{\infty}\mathbf{C}_n\cos(\beta_n x)+\mathbf{U}_0^*=0,\quad 0<x<a,\quad b<x<d. \tag{45}$$

Eqs. (44) and (45) form the triple trigonometric series equations with respect to $\mathbf{C}_n$.

In what follows the triple series Eqs. (44) and (45) will be converted into a singular integral equation. For this purpose, we first introduce the dislocation density function $\mathbf{F}(x,p)$ in the Laplace domain as

$$\mathbf{F}(x,p)=\frac{\partial\Delta\mathbf{U}^*(x,0,p)}{2\partial x}. \tag{46}$$

By virtue of the finite Fourier transform, we can choose $\mathbf{C}_n$ as a finite Fourier sine integral

$$\mathbf{C}_n=-\frac{2}{\beta_n d}\int_a^b\mathbf{F}(u,p)\sin(\beta_n u)\mathrm{d}u. \tag{47}$$

Substituting Eq. (47) into Eq. (44) and noting the intrinsic properties of $\mathbf{Q}_n$ as n tends to infinity, i.e.,

$$\mathbf{Q}_n\to\beta_n\left(\boldsymbol{\Omega}_1\mathbf{M}_1^{-1}\mathbf{M}_2+\boldsymbol{\Omega}_2\right)^{-1},\quad n\to\infty, \tag{48}$$

we can finally obtain a singular integral equation of the first kind as follows:

$$\frac{1}{d}\int_a^b\frac{\sin(\pi u/d)}{\cos(\pi x/d)-\cos(\pi u/d)}\mathbf{F}(u,p)\mathrm{d}u+\frac{1}{d}\int_a^b\mathbf{X}(u,x,p)\mathbf{F}(u,p)\mathrm{d}u=-\frac{1}{p}\mathbf{S}_0(x),a<x<b, \tag{49}$$

where

$$\mathbf{X}(u,x,p)=2\sum_{n=1}^{\infty}\left\{\frac{1}{\beta_n}(\boldsymbol{\Omega}_1\mathbf{M}_1^{-1}\mathbf{M}_2+\boldsymbol{\Omega}_2)\mathbf{Q}_n-\mathbf{I}\right\}\sin(\beta_n u)\cos(\beta_n x), \tag{50}$$

$$\mathbf{S}_0=\boldsymbol{\Gamma}^{-1}\boldsymbol{\tau}_0, \tag{51}$$

with

$$\boldsymbol{\Gamma}=2\mathbf{M}_2\left(\boldsymbol{\Omega}_1\mathbf{M}_1^{-1}\mathbf{M}_2+\boldsymbol{\Omega}_2\right)^{-1}, \tag{52}$$

and $\mathbf{I}$ being the 3×3 identity matrix. It should be pointed out that in the derivation of Eq. (49), the following relation

$$\sum_{n=1}^{\infty}\sin(nu)\cos(nx)=\frac{1}{2}\frac{\sin(u)}{\cos(x)-\cos(u)}, \tag{53}$$

has been used.

On the other hand, substituting Eq. (47) into Eq. (45), and recalling the known result

$$\frac{u}{2}+\sum_{n=1}^{\infty}\frac{1}{n}\sin(nu)\cos(nx)=\begin{cases}\pi/2, & 0<x<u,\\ \pi/4, & u=x,\\ 0, & u<x<\pi,\end{cases} \tag{54}$$

$\mathbf{U}_0^*(p)$ can be solved as

$$\mathbf{U}_0^*=-\frac{2}{d}\int_a^b u\mathbf{F}(u,p)\mathrm{d}u. \tag{55}$$

Introducing the following normalized quantities:

$$u = \frac{d}{\pi}\arccos\left\{\eta\left(\cos\frac{\pi b}{d} - \cos\frac{\pi a}{d}\right)/2 + \left(\cos\frac{\pi b}{d} + \cos\frac{\pi a}{d}\right)/2\right\}, \quad -1 < (\eta, \varsigma) < 1, \tag{56}$$

$$x = \frac{d}{\pi}\arccos\left\{\varsigma\left(\cos\frac{\pi b}{d} - \cos\frac{\pi a}{d}\right)/2 + \left(\cos\frac{\pi b}{d} + \cos\frac{\pi a}{d}\right)/2\right\}, \quad -1 < (\eta, \varsigma) < 1, \tag{57}$$

Eq. (49) can be rewritten as a standard singular Cauchy integral equation over $(-1, 1)$:

$$\frac{1}{\pi}\int_{-1}^{1}\frac{1}{\eta-\varsigma}\overline{\mathbf{F}}(\eta,p)\mathrm{d}\eta + \frac{1}{\pi}\int_{-1}^{1}\mathbf{T}(\eta,\varsigma,p)\overline{\mathbf{F}}(\eta,\mathbf{p})\mathbf{du} = -\frac{1}{p}\overline{\mathbf{S}}_0, \quad -1 < \varsigma < 1, \tag{58}$$

where

$$\overline{\mathbf{F}}(\eta,p) = \mathbf{F}(u,p), \tag{59}$$

$$\mathbf{T}(\eta,\xi,p) = -\left(\cos\frac{\pi b}{d} - \cos\frac{\pi a}{d}\right)\Big/\left(2\sin\frac{\pi u}{d}\right)\mathbf{X}(u,x,p), \tag{60}$$

$$\overline{\mathbf{S}}_{\mathbf{0}}(\varsigma,\mathbf{p}) = \mathbf{S}_{\mathbf{0}}(\mathbf{x},\mathbf{p}). \tag{61}$$

Applying the numerical method proposed by Erdogan and Gopta [25], the Cauchy singular integral Eq. (58) together with the corresponding single-valued condition

$$\int_{-1}^{1}\overline{\mathbf{F}}(\eta,p)\mathrm{d}\eta = 0, \tag{62}$$

can further be transformed into a system of linear algebraic equations as follows:

$$\sum_{j=1}^{K}\left(\frac{1}{\eta_j-\varsigma_i}\mathbf{I} + \mathbf{T}(\eta_j,\varsigma_i,p)\right)\frac{\mathbf{Y}^*(\eta_j,p)}{K} = -\frac{1}{p}\bar{\mathbf{S}}_0(\varsigma_i), \tag{63}$$

$$\sum_{j=1}^{K}\frac{\mathbf{Y}^*(\eta_j,p)}{K} = 0, \tag{64}$$

where $\mathbf{Y}^*(\eta,p) = \sqrt{1-\eta^2}\overline{\mathbf{F}}(\eta,p)$, $\eta_j = \cos[(2j-1)\pi/2K]$, $j = 1, 2, \ldots, K$, $\varsigma_i = \cos(i\pi/K)$, $i = 1, 2, \ldots, K-1$, and K is the total discrete points of η.

Finally, the Laplace inversion of $\mathbf{Y}^*(\eta,p)$, i.e., $\mathbf{Y}(\eta,t)$ is easily obtained by employing some well known numerical methods.

It is worth remarking that the present solution for the coupled magneto-electro-elastic solid contains the solutions for various reduced cases (by setting the coupling coefficients to zero). In particular, it can be reduced to the solution to the problem where a dynamic anti-plane interfacial crack is between two dissimilar piezoelectric plates, which in fact has not been solved so far.

3.2. Field intensity factors and energy release rate

The dynamic stress intensity factors (DSIFs), dynamic electric displacement intensity factors (DEDIFs) and dynamic magnetic induction intensity factors (DMIIFs) in vector form $\mathbf{K}_\Lambda = [K_{T\Lambda} \quad K_{D\Lambda} \quad K_{B\Lambda}]^{\mathrm{T}}(\Lambda = b, a)$ in the time domain at the two crack tips are defined and easily derived as

$$\mathbf{K}_{b(t)} = \lim_{x\to b}\sqrt{2\pi(x-b)}\mathbf{T}_{y2}(x,0,t) = -\sqrt{\frac{d}{2}\left(\cos\frac{\pi a}{d}\Big/\sin\frac{\pi b}{d} - \cot\frac{\pi b}{d}\right)}\mathbf{\Gamma}Y(1,t), \tag{65}$$

$$\mathbf{K}_{a(t)} = \lim_{x\to a}\sqrt{2\pi(a-x)}\mathbf{T}_{y2}(x,0,t) = \sqrt{\frac{d}{2}\left(\cot\frac{\pi a}{d} - \cos\frac{\pi b}{d}\Big/\sin\frac{\pi a}{d}\right)}\mathbf{\Gamma}Y(-1,t). \tag{66}$$

It is interesting to point out that the coefficients in the field intensity factors $\mathbf{K}_b$ and $\mathbf{K}_a$ differ from the known expressions of the dynamic field intensity factors for magneto-electro-elastic materials [22], and from those of the static field intensity factors of a crack at an arbitrary position of a homogeneous piezoelectric rectangle [26]. The reason for this difference is that, in the present work, two novel normalized quantities, i.e., Eqs. (56) and (57), are introduced in order to reduce Eq. (49) to a standard singular Cauchy integral equation.

For the magneto-electrically impermeable cracks, the DERRs are very important to evaluate the behaviors of crack tips. In accordance with the definition of the energy release rates proposed by Pak [27], the DERRs can finally be expressed as

$$G_b(t) = \frac{1}{2}\mathbf{K}_b^{\mathrm{T}}(t)\mathbf{\Gamma}^{-1}\mathbf{K}_b(t) = \frac{d}{4}\left(\cos\frac{\pi a}{d}\Big/\sin\frac{\pi b}{d} - \cot\frac{\pi b}{d}\right)\mathbf{Y}^{\mathrm{T}}(1,t)\mathbf{\Gamma}^{\mathrm{T}}\mathbf{Y}(1,t), \tag{67}$$

$$G_a(t) = \frac{1}{2}\mathbf{K}_a^{\mathrm{T}}(t)\mathbf{\Gamma}^{-1}\mathbf{K}(t)_a = \frac{d}{4}\left(\cot\frac{\pi a}{d} - \cos\frac{\pi b}{d}\Big/\sin\frac{\pi a}{d}\right)\mathbf{Y}^{\mathrm{T}}(-1,t)\mathbf{\Gamma}^{\mathrm{T}}\mathbf{Y}(-1,t). \tag{68}$$

It should be noted that the expressions of DERRs given above are, in fact, the same as those for an impermeable crack in homogeneous magneto-electro-elastic materials [14], and that if all the coupled magnetic coefficients are set to zero, then the expressions are essentially agreement with those for an interfacial crack between two dissimilar piezoelectric strips [28].

Further analysis on Eqs. (65)–(68) shows that both the field intensity factors and DERRs of interfacial cracks are related to the material parameters, crack configuration, as well as all the mechanical, electrical and magnetic loadings.

It is easy to know that for a homogeneous magneto-electro-elastic plate, the corresponding linear algebraic equations in Laplace domain can be obtained from Eqs. (63) and (64) as

$$\frac{1}{K}\sum_{j=1}^{K}\frac{1}{\eta_j-\varsigma_i}\mathbf{\Xi}\mathbf{Y}^*(\eta_j,p) + \frac{1}{K}\sum_{j=1}^{K}\mathbf{R}(\eta,\varsigma,p)\mathbf{Y}^*(\eta_j,p) = -\frac{1}{p}\boldsymbol{\tau}_0, \tag{69}$$

$$\frac{1}{K}\sum_{j=1}^{K}\mathbf{\Xi}\mathbf{Y}^*(\eta_j,p) = 0, \tag{70}$$

where $\mathbf{\Xi} = \mathbf{\Xi}_1 = \mathbf{\Xi}_2, \mathbf{R}(\eta,\varsigma,p)$ are given in Appendix C.

Following the same procedure as in [22], the DSIFs in time domain can be written as

$$K_{T_b}(t) = -\sqrt{\frac{d}{2}\left(\cos\frac{\pi a}{d}\Big/\sin\frac{\pi b}{d} - \cot\frac{\pi b}{d}\right)}\,\Psi(1,t), \tag{71}$$

$$K_{T_a}(t) = \sqrt{\frac{d}{2}\left(\cot\frac{\pi a}{d} - \cos\frac{\pi b}{d}\Big/\sin\frac{\pi a}{d}\right)}\,\Psi(-1,t), \tag{72}$$

where

$$\Psi(\eta,t) = \frac{1}{2\pi\mathrm{i}}\int_{\mathrm{Br}}[c_{44}\quad e_{15}\quad f_{15}]\mathbf{Y}^*(\eta,p)\mathrm{e}^{pt}\,\mathrm{d}p. \tag{73}$$

The DEDIFs and DMIIFs in time domain can be described as

$$\begin{bmatrix}K_{Db}(t)\\ K_{Bb}(t)\end{bmatrix} = -\sqrt{\frac{d}{2}\left(\cos\frac{\pi a}{d}\Big/\sin\frac{\pi b}{d} - \cot\frac{\pi b}{d}\right)}\,\Phi(1)H(t)\begin{bmatrix}D_0\\ B_0\end{bmatrix}, \tag{74}$$

$$\begin{bmatrix}K_{Da}(t)\\ K_{Ba}(t)\end{bmatrix} = \sqrt{\frac{d}{2}\left(\cot\frac{\pi a}{d} - \cos\frac{\pi b}{d}\Big/\sin\frac{\pi a}{d}\right)}\,\Phi(-1)H(t)\begin{bmatrix}D_0\\ B_0\end{bmatrix}, \tag{75}$$

where $\Phi(\eta)$ satisfies the following algebra equation

$$\sum_{j=1}^{K}\left(\frac{1}{\eta_j-\varsigma_i} + \frac{\cos\frac{\pi a}{d} - \cos\frac{\pi b}{d}}{\sin\frac{\pi u(\eta)}{d}}\sum_{n=1}^{\infty}(2\alpha_{2n}-1)\sin(\beta_n u(\eta))\cos(\beta_n x(\varsigma))\right)\frac{\Phi(\eta_j)}{K} = -1, \tag{76}$$

$$\sum_{j=1}^{K}\frac{\Phi(\eta_j)}{K}=0, \tag{77}$$

with α_{2n} being given in Appendix C. Correspondingly, the DERRs in time domain are simplified as

$$G_{\wp}=\frac{1}{2}\mathbf{K}_{\wp}^{\mathrm{T}}\boldsymbol{\Xi}^{-1}\mathbf{K}_{\wp},\quad \wp=b,a. \tag{78}$$

As shown in Eqs. (71) and (72), similar to interfacial cracks, the DSIFs for homogeneous plate are related to the mechanical loadings, electrical loadings, magnetic loadings and the relevant material properties. However, from Eqs. (74) and (75), it is easy to observe that different to the interfacial crack case, both DEDIFs and DMIIFs for the homogeneous plate are the Heaviside unit step function of time, and are only related to the corresponding electrical or magnetic impact loadings; they are independent of the mechanical loadings and the relevant material properties. It should be pointed out that these phenomena are similar to those for the impact crack problems of functionally graded magneto-electro-elastic strip [22].

4. Effects of crack surface conditions on the field intensity factors and DERRs

The magneto-electrically impermeable interfacial crack (Case 1) has been considered in Section 3. Similarly, the singular integral equations and corresponding single-valued conditions for the other cases of interfacial cracks can be derived as

Case 2:

$$\begin{aligned}&\frac{1}{d}\int_a^b\frac{\sin(\pi u/d)}{\cos(\pi x/d)-\cos(\pi u/d)}\begin{bmatrix}F^{(1)}(u,p)\\F^{(3)}(u,p)\end{bmatrix}\mathrm{d}u\\&\quad+\frac{1}{d}\int_a^b\begin{bmatrix}X^{(1,1)}(u,x,p)&X^{(1,3)}(u,x,p)\\X^{(3,1)}(u,x,p)&X^{(3,3)}(u,x,p)\end{bmatrix}\begin{bmatrix}F^{(1)}(u,p)\\F^{(3)}(u,p)\end{bmatrix}\mathrm{d}u\\&=-\frac{1}{p}\begin{bmatrix}S_0^{(1)}\\S_0^{(3)}\end{bmatrix},\quad a<x<b,\end{aligned} \tag{79}$$

$$\int_a^b\begin{bmatrix}F^{(1)}(u,p)\\F^{(3)}(u,p)\end{bmatrix}\mathrm{d}u=0. \tag{80}$$

Case 3:

$$\begin{aligned}&\frac{1}{d}\int_a^b\frac{\sin(\pi u/d)}{\cos(\pi x/d)-\cos(\pi u/d)}\begin{bmatrix}F^{(1)}(u,p)\\F^{(2)}(u,p)\end{bmatrix}\mathrm{d}u\\&\quad+\frac{1}{d}\int_a^b\begin{bmatrix}X^{(1,1)}(u,x,p)&X^{(1,2)}(u,x,p)\\X^{(2,1)}(u,x,p)&X^{(2,2)}(u,x,p)\end{bmatrix}\begin{bmatrix}F^{(1)}(u,p)\\F^{(2)}(u,p)\end{bmatrix}\mathrm{d}u=-\frac{1}{p}\begin{bmatrix}S_0^{(1)}\\S_0^{(2)}\end{bmatrix},\quad a<x<b,\end{aligned} \tag{81}$$

$$\int_a^b\begin{bmatrix}F^{(1)}(u,p)\\F^{(2)}(u,p)\end{bmatrix}\mathrm{d}u=0. \tag{82}$$

Case 4:

$$\begin{aligned}&\frac{1}{d}\int_a^b\frac{\sin(\pi u/d)}{\cos(\pi x/d)-\cos(\pi u/d)}F^{(1)}(u,p)\mathrm{d}u\\&\quad+\frac{1}{d}\int_a^b X^{(1,1)}(u,x,p)F^{(1)}(u,p)\mathrm{d}u=-\frac{1}{p}S_0^{(1)},\quad a<x<b,\end{aligned} \tag{83}$$

$$\int_a^b F^{(1)}(u,p)\mathrm{d}u=0, \tag{84}$$

where the quantities with superscript $(i,j)(i,j = 1,2,3)$ represent the elements of the ith row and jth column in the corresponding matrix.

These equations corresponding to different crack surface conditions can further be solved by the method discussed in Section 3. Thus, the field intensity factors and DERRs can finally be derived as

Case 2:

$$\mathbf{K}_b(t) = -\sqrt{\frac{d}{2}\left(\cos\frac{\pi a}{d}\Big/\sin\frac{\pi b}{d} - \cot\frac{\pi b}{d}\right)}\begin{bmatrix} \Gamma^{(1,1)} & \Gamma^{(1,3)} \\ \Gamma^{(2,1)} & \Gamma^{(2,3)} \\ \Gamma^{(3,1)} & \Gamma^{(3,3)} \end{bmatrix}\begin{bmatrix} Y^{(1)}(1,t) \\ Y^{(3)}(1,t) \end{bmatrix}, \tag{85}$$

$$\mathbf{K}_a(t) = \sqrt{\frac{d}{2}\left(\cot\frac{\pi a}{d} - \cos\frac{\pi b}{d}\Big/\sin\frac{\pi a}{d}\right)}\begin{bmatrix} \Gamma^{(1,1)} & \Gamma^{(1,3)} \\ \Gamma^{(2,1)} & \Gamma^{(2,3)} \\ \Gamma^{(3,1)} & \Gamma^{(3,3)} \end{bmatrix}\begin{bmatrix} Y^{(1)}(-1,t) \\ Y^{(3)}(-1,t) \end{bmatrix}, \tag{86}$$

$$G_\wp(t) = \frac{1}{2}[K_{T\wp}(t)K_{B\wp}(t)]\begin{bmatrix} \Gamma^{(1,1)}\Gamma^{(1,3)} \\ \Gamma^{(3,1)}\Gamma^{(3,3)} \end{bmatrix}^{-1}\begin{bmatrix} K_{T\wp}(t) \\ K_{B\wp}(t) \end{bmatrix}, \quad \wp = b, a, \tag{87}$$

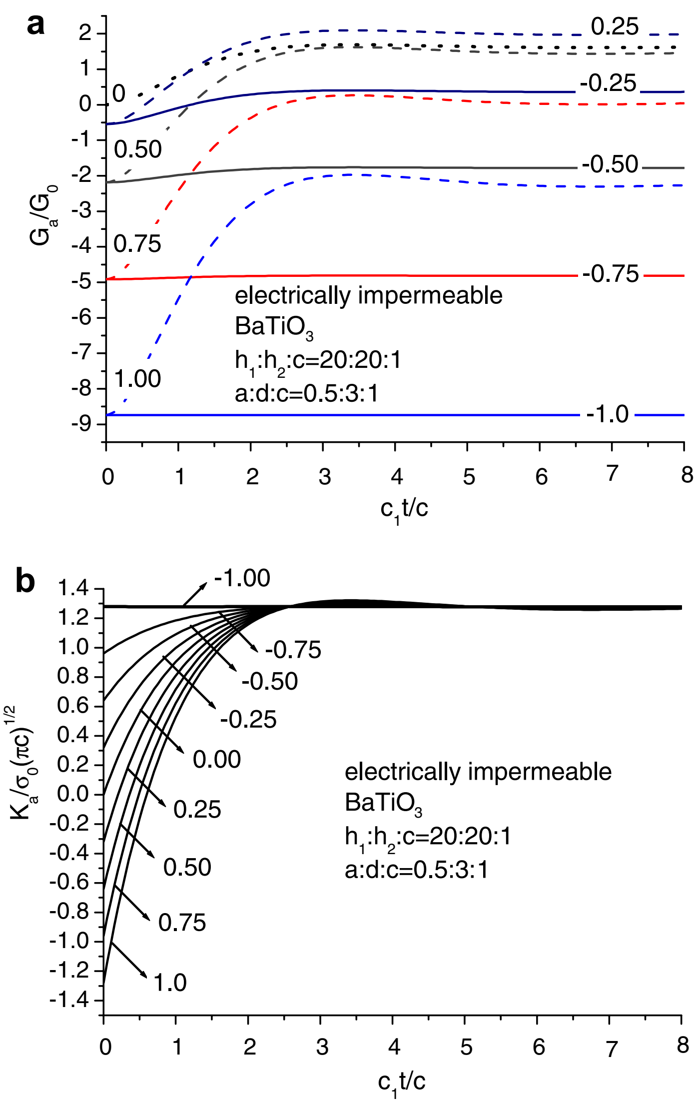

Fig. 2. Normalized (a) DERRs and (b) DSIFs of an electrically impermeable central crack in a homogeneous piezoelectric plate for different electrical loadings λ_D with both h_1 and h_2 approaching to infinite.

Case 3:

$$\mathbf{K}_b(t) = -\sqrt{\frac{d}{2}\left(\cos\frac{\pi a}{d} / \sin\frac{\pi b}{d} - \cot\frac{\pi b}{d}\right)} \begin{bmatrix} \Gamma^{(1,1)} & \Gamma^{(1,2)} \\ \Gamma^{(2,1)} & \Gamma^{(2,2)} \\ \Gamma^{(3,1)} & \Gamma^{(3,2)} \end{bmatrix} \begin{bmatrix} Y^{(1)}(1,t) \\ Y^{(2)}(1,t) \end{bmatrix}, \tag{88}$$

$$\mathbf{K}_a(t) = \sqrt{\frac{d}{2}\left(\cot\frac{\pi a}{d} - \cos\frac{\pi b}{d} / \sin\frac{\pi a}{d}\right)} \begin{bmatrix} \Gamma^{(1,1)} & \Gamma^{(1,2)} \\ \Gamma^{(2,1)} & \Gamma^{(2,2)} \\ \Gamma^{(3,1)} & \Gamma^{(3,2)} \end{bmatrix} \begin{bmatrix} Y^{(1)}(-1,t) \\ Y^{(2)}(-1,t) \end{bmatrix}, \tag{89}$$

$$G_\wp(t) = \frac{1}{2}[K_{T\wp}(t) K_{D\wp}(t)] \begin{bmatrix} \Gamma^{(1,1)} & \Gamma^{(1,2)} \\ \Gamma^{(2,1)} & \Gamma^{(2,2)} \end{bmatrix}^{-1} \begin{bmatrix} K_{T\wp}(t) \\ K_{D\wp}(t) \end{bmatrix}, \quad \wp = b, a, \tag{90}$$

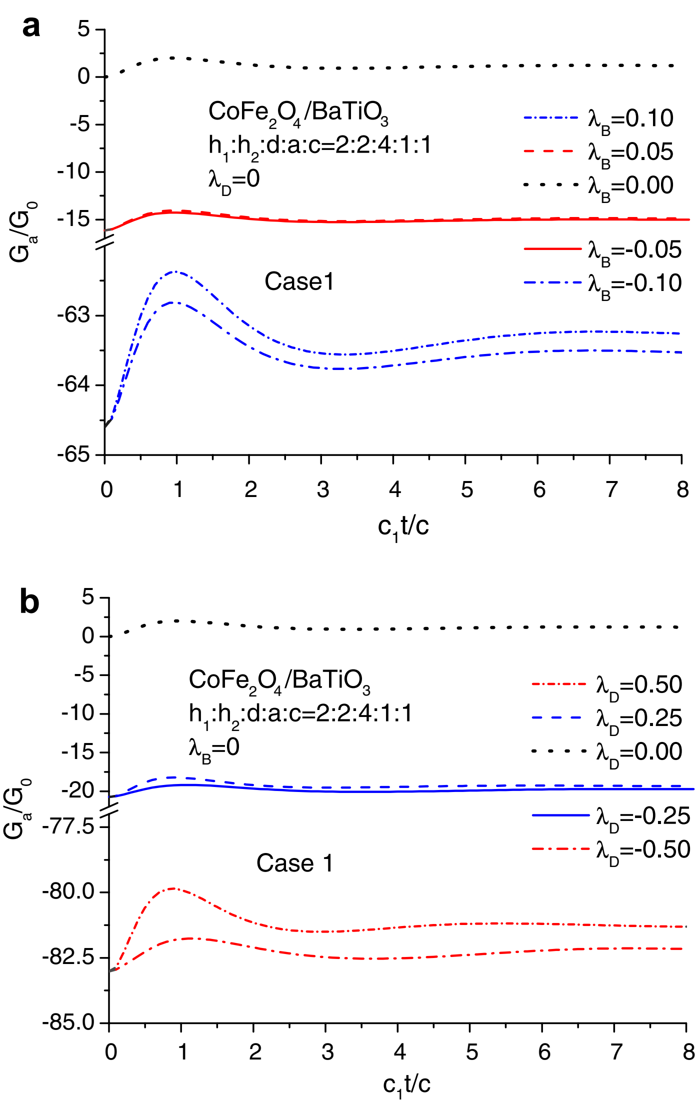

Fig. 3. Normalized DERRs of a magneto-electrically impermeable central crack versus normalized time for (a) different magnetic impact loadings with $\lambda_D = 0.0$ and for (b) different electrical impact loadings with $\lambda_B = 0.0$.

Case 4:

$$\mathbf{K}_b(t) = -\sqrt{\frac{d}{2}\left(\cos\frac{\pi a}{d} / \sin\frac{\pi b}{d} - \cot\frac{\pi b}{d}\right)} \begin{bmatrix} \Gamma^{(1,1)} \\ \Gamma^{(2,1)} \\ \Gamma^{(3,1)} \end{bmatrix} Y^{(1)}(1,t), \tag{91}$$

$$\mathbf{K}_a(t) = \sqrt{\frac{d}{2}\left(\cot\frac{\pi a}{d} - \cos\frac{\pi b}{d} / \sin\frac{\pi a}{d}\right)} \begin{bmatrix} \Gamma^{(1,1)} \\ \Gamma^{(2,1)} \\ \Gamma^{(3,1)} \end{bmatrix} Y^{(1)}(-1,t), \tag{92}$$

$$G_\wp(t) = \frac{1}{2\Gamma^{(1,1)}} K_{T\wp}^2(t), \quad \wp = b, a. \tag{93}$$

The analysis above implies that for the magnetically (or electrically) permeable interfacial crack, the applied magnetic (or electrical) loadings have no influence on the fracture behaviors of the crack tips, and that the DMIIFs (or DEDIFs) can be described as a function of DSIFs and DEDIFs (or DMIIFs). Moreover, for magnetically (or electrically) permeable interfacial cracks, the DERRs are functions of the DSIFs and

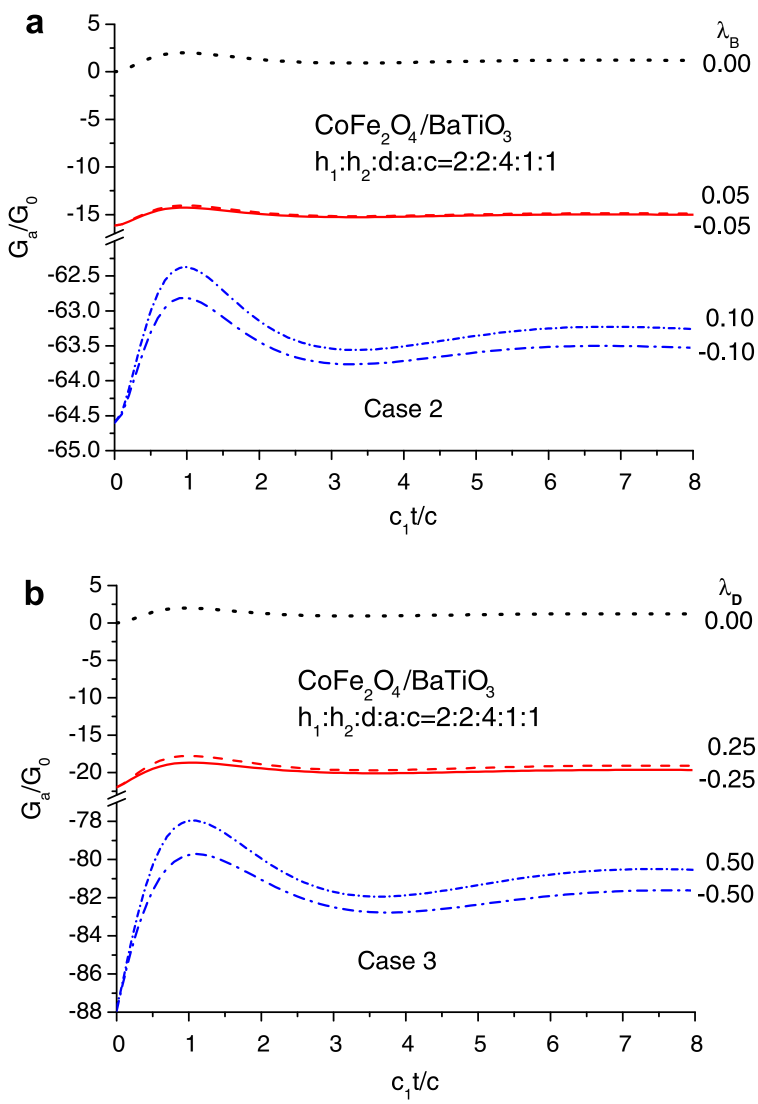

Fig. 4. Normalized DERRs versus normalized time for (a) different magnetic impact loadings in Case 2 and for (b) different electrical impact loadings in Case 3.

DEDIFs (or DMIIFs) only. Thus, for the magneto-electrically permeable case, the DEDIFs, DMIIFs and DERRs are all the functions of the corresponding DSIFs (just as shown in Eqs. (91)–(93)). Therefore, for magneto-electrically permeable cracks, the DERRs and DSIFs are quite equivalent to the fracture parameters, which has been observed for unbounded magneto-electro-elastic materials (see e.g., [11] or [13]).

It is worth pointing out that for homogeneous magneto-electro-elastic plate with an internal crack, the results (omitted here) corresponding to Cases 2–4 can further be obtained easily.

5. Numerical examples and discussions

In this section, numerical calculations are further carried out to show the effects of the crack configuration and loading combination parameters on the normalized DERRs. Without loss of generality, in all our numerical procedure, σ_0 is taken as 4.2×10^6 N/m^2, and G_0 as $\pi c \sigma_0^2/(2m_{11})$, corresponding to the static energy release rate for an infinite magneto-electro-elastic plane containing a magneto-electrically impermeable crack of length $2c = b - a$ under anti-plane shear loadings. The normalized time is taken as $c_1 t/c$ where c_1, as pointed out before, is the "extended" shear wave speed of the upper plate.

For comparison with the known results, as a special example, both materials 1 and 2 are taken as piezoelectric ceramics $BaTiO_3$ with the material properties being taken from [29]. We also set $h_1 = h_2$ and $a{:}d{:}c = 0.5{:}3{:}1$ and assume that the crack is electrically impermeable. Thus, the dynamic crack problem corresponding to $h_2/c \to \infty$ form an electrically impermeable central crack problem of piezoelectric strip with the crack perpendicular to the boundaries of the finite strip, which has been considered by Wang and Yu [29] in detail. Comparing the normalized DERRs, i.e., Fig. 2a with Fig. 5 in [29] and normalized DSIFs, i.e., Fig. 2b with Fig. 4 in [29], it is easily seen that the present results are the same as those given in [29]. It should be pointed out that λ_D in Fig. 2 has the same meaning as in [29], i.e., $\lambda_D = D_0 e_{15}^2/(\sigma_0 \varepsilon_{11}^2)$ representing the electric loading combination parameter.

As an application, the effects of magnetic and/or electrical impact loadings on the fracture behaviors of an interfacial crack with magnetically and/or electrically impermeable crack surface conditions (Cases 1–3) for the combination of $CoFe_2O_4/BaTiO_3$ are then examined in this section. The material properties of $CoFe_2O_4$ and $BaTiO_3$ are the same as those given in [15] or in [19]. Numerical results are respectively plotted in Figs. 3–5, where λ_D is again the combination parameter and $\lambda_B = B_0 f_{15}^1/(\sigma_0 \mu_{11}^1)$ is a newly introduced loading combination parameter (see e.g., [19]). From these figures, it is easily observed that for the present problem, the oscillation peak occurs, and that the effects of crack configuration (including both the crack position and geometry criterion of the plate) on the times for the DERRs reaching the corresponding peak values are more evident than those of both magnetic and electrical loadings. As shown in Figs. 3 and 4, for a given electrical loading,

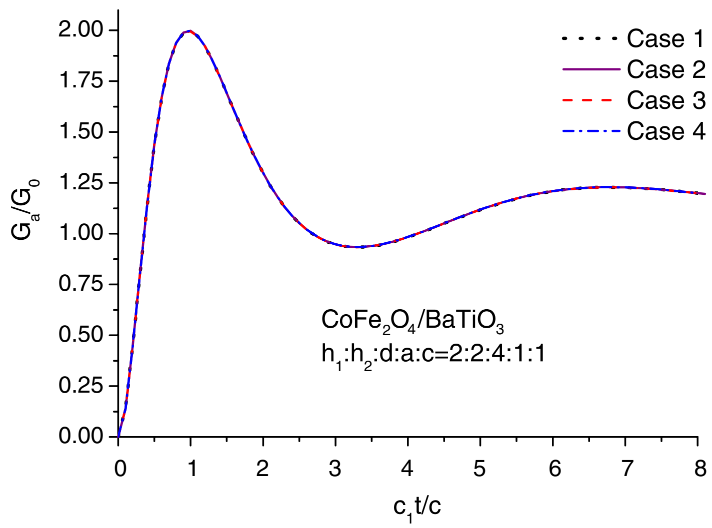

Fig. 5. Normalized DERRs versus normalized time for different crack surface conditions under an anti-plane shear impact loading.

Table 1
Comparison of normalized DERRs of a central crack under different crack surface conditions for the combined $CoFe_2O_4/BaTiO_3$ under the anti-plane shear impact loading

	c_1t/c														
	0.1	0.2	0.3	0.4	0.5	0.6	0.7	0.8	0.9	1.0	1.1	1.2	1.3	1.4	1.5
Ga/G_0															
Case 1	0.13772	0.44233	0.7996	1.143	1.4376	1.6686	1.8337	1.9375	1.9885	1.9963	1.9706	1.9201	1.8526	1.7745	1.6909
Case 2	0.13793	0.44295	0.80062	1.1443	1.4391	1.6701	1.8352	1.9389	1.9898	1.9974	1.9715	1.9209	1.8533	1.7751	1.6915
Case 3	0.13787	0.44279	0.80033	1.1439	1.4384	1.6693	1.8342	1.9378	1.9886	1.9961	1.9701	1.9195	1.8519	1.7737	1.6901
Case 4	0.13793	0.44296	0.80063	1.1444	1.4391	1.6702	1.8352	1.939	1.9899	1.9976	1.9717	1.9211	1.8535	1.7753	1.6916

$CoFe_2O_4/BaTiO_3$: $\lambda_D = \lambda_B = 0.0$, h_1: h_2:d:a:c = 2:2:4:1:1.

the algebraic value of DERRs decreases with increasing magnitude of the magnetic loadings. Similarly, for a given magnetic loading, the algebraic value of DERRs decreases with increasing magnitude of electrical loadings. This observation indicates that both the magnetic and electrical impact loadings impede crack propagation and growth. Figs. 3 and 4 also implies that, for $CoFe_2O_4/BaTiO_3$ combination, although the (algebraic) DERRs for a negative magnetic (or electrical) impact loading are slightly smaller than those for the corresponding positive magnetic (or electrical) loading, the impact loading directions (positive or negative) have only slight influence on the crack extension force of interfacial cracks, particularly for a small value of $|\lambda_B|$ (or $|\lambda_D|$). Moreover, just as shown in Fig. 5 and Table 1 (Table 1 gives partial numerical results plotted in Fig. 5 for clarity), the four kinds of ideal crack surface conditions (Cases 1–4) have nearly no effect on the DERRs under only anti-plane shear impact loading.

In what follows, we evaluate the effect of the crack configuration on the dynamic fracture behaviors of the crack tips. As pointed out before, the magneto-electrically permeable crack surface assumption is perhaps more reasonable for mode III crack problems, therefore numerical results are only plotted graphically for Case 4. The effect of the crack position on the DERRs for an internal crack is illustrated in Fig. 6 where $e_y = \frac{h_1-h_2}{h_1+h_2}(-1 < e_y < 1)$ and $e_x = -1 - 2a/(d-2c)|(0 \leqslant e_x < 1)$ represent the eccentricities away from the horizontal and vertical mid-planes, respectively. The effects of plate size on the normalized DERRs are shown in Figs. 7 and 8, respectively.

From Fig. 6a, it is observed that for an interfacial crack centered at the vertical mid-plane (i.e., $e_x = 0$), the DERRs, in general, increase with increasing $|e_y|$. Thus, the interfacial crack with equal distances to the top and bottom surfaces (*i.e.*,$h_1 = h_2$) can be approximately thought as most stable. In addition, it is worth noting that for a e_y-pair (e.g., $e_y = -0.85$ and $e_y = 0.85$), the eccentricity corresponding to the negative value of e_y enhances the interfacial crack propagation more than the one corresponding to the positive value of e_y. On the other hand, as shown in Fig. 6b, the eccentricity away from the vertical mid-plane can also enhance crack propagate and grow. Moreover, the crack propagation and growth always occurs at the crack tip closer to the flank surfaces of the plate. As expected from Figs. 7 and 8, for a central interfacial crack, increasing the width and height of the plate decreases the DERRs. In addition, Fig. 8 indicates that the curves of the normalized DERRs corresponding to $h_1/c = 2$ and 10 are very close to each other. Therefore, when the height of the piezomagnetic (or piezoelectric) layer exceeds the crack length, its effect on the DERRs becomes negligible. Finally, we remark that our numerical results (omitted here) also illustrate that the crack position and/or crack configuration have the same effects on the DERRs of crack tips of the interfacial crack under other crack surface conditions (i.e., Cases 1–3).

6. Conclusions

In this paper, the dynamic fracture behaviors of an interfacial crack between two bonded magneto-electro-elastic plates under anti-plane mechanical loadings and in-plane magnetic and electrical loadings are investigated. Four kinds of crack surface conditions are adopted. The interfacial crack is assumed to be at an arbitrary position. Finite Fourier transform method and dislocation density functions are used to reduce the mixed boundary value problem to a standard singular Cauchy integral equation, which is further solved numerically. The field intensity factors and DERRs are obtained and analyzed. The effects of both the applied impact loadings and crack configurations on the DERRs are shown graphically. The main results are as follows.

- Finite Fourier transform method and singular integral equation technique can be used to solve the transient response problems of mode III interfacial crack. The crack is assumed to be at an arbitrary position on the interface between the two bonded magneto-electro-elastic plates.
- Crack configuration including the position and relative criterion of the cracks has a more evident effect on the time for the DERR reaching its peak value than magnetic and/or electrical impact loadings.
- Different to an internal crack embedded in a homogeneous magneto-electro-elastic plate, both the field intensity factors and DERRs of an interfacial crack are not only related to the crack configuration but also related to the material parameters. Furthermore, for a magneto-electrically impermeable interfacial crack, both the field intensity factors and DERRs depend on the applied mechanical, magnetic and electrical loadings simultaneously.

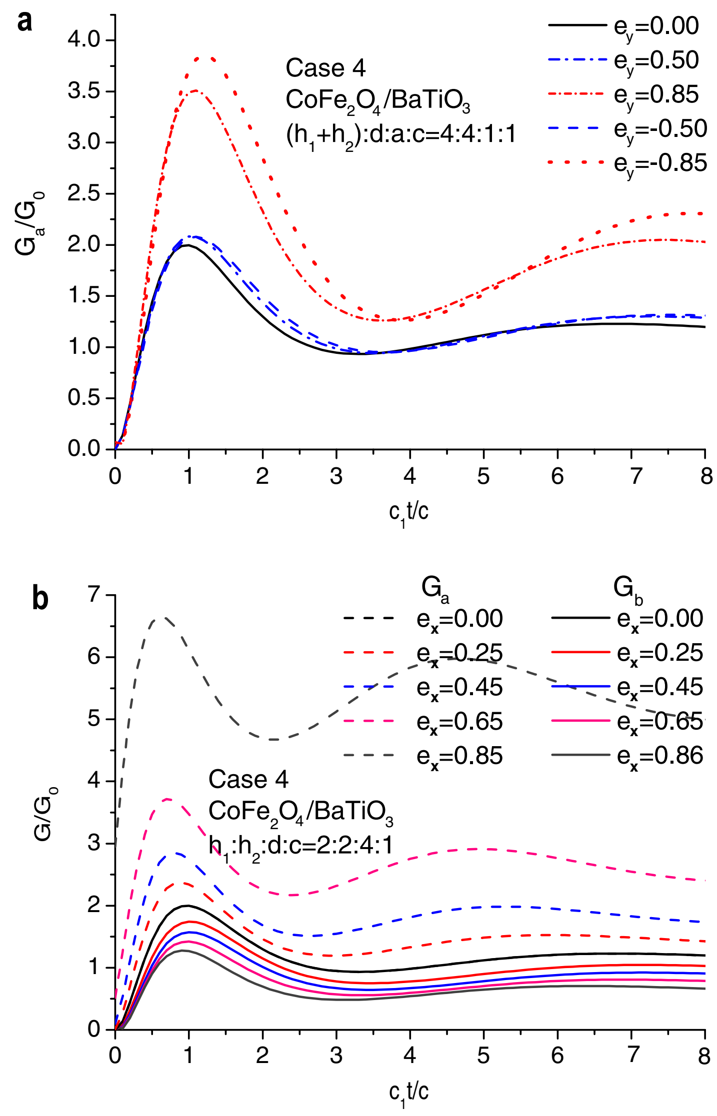

Fig. 6. Normalized DERRs of a magneto-electrically permeable internal crack versus normalized time for different (a) $e_y = (h_1 - h_2)/(h_1 + h_2)$ and (b) $e_x = |1 - 2a/(d - 2c)|$ where c is the half length of the crack and d the total width of the plate, under anti-plane shear impact loading.

- The magnetic (or electrical) impact loadings have no influence on the fracture behaviors for magnetically (or electrically) permeable interfacial cracks according to maximum energy release rate criterion. On the other hand, magnetic (or electrical) impact loadings always impede the crack propagation and growth for magnetically (or electrically) impermeable interfacial cracks, and the directions of both magnetic and electrical impact loadings have no apparent effect on the crack extension force.
- For $CoFe_2O_4/BaTiO_3$ combination, under only anti-plane shear impact loadings, the DERRs corresponding to the four kinds of ideal crack surface conditions considered here are almost the same for a given crack configuration.
- For fixed width and total height of the composite plate and length of the crack, the eccentricity away from either the horizontal mid-plane or vertical mid-plane can enhance the crack propagation. For fixed crack length and crack position, increasing the width and height of the bonded plate can impede the crack propagation and growth.

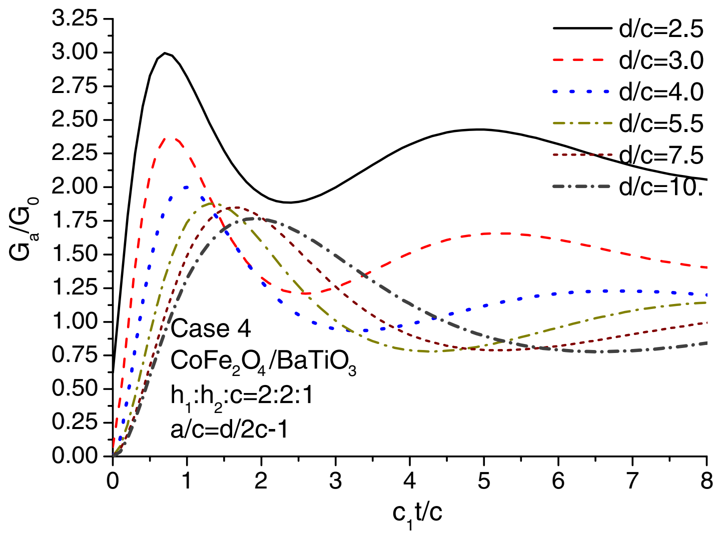

Fig. 7. Normalized DERRs of a magneto-electrically permeable central crack versus normalized time for different ratio d/c where c is the half length of the crack and d total width of the plate, under anti-plane shear impact loading.

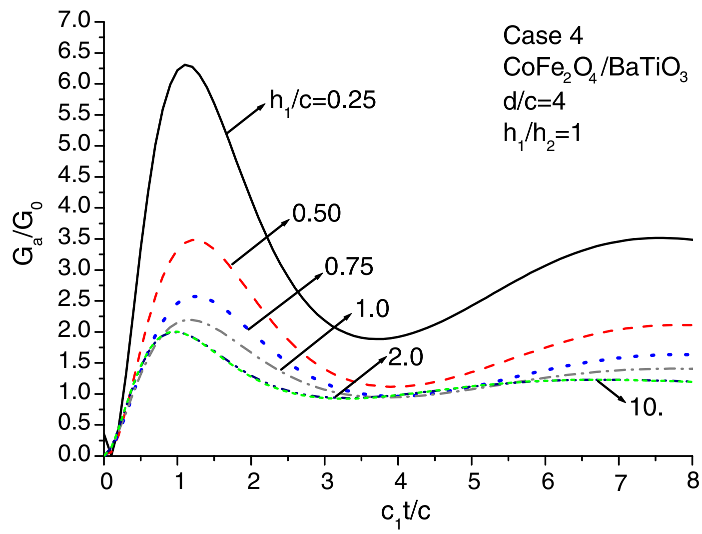

Fig. 8. Normalized DERRs of a magneto-electrically permeable central crack versus normalized time for different heights of the plate under an anti-plane shear impact loading.

Acknowledgement

The work was supported by Natural Science Fund of China, Natural Science Fund of Hebei Province, China, and AFOSR/AFRL.

Appendix A

a_{1i}, b_{1i}, c_{1i}, a_{2i}, b_{2i} and c_{2i} in Eq. (8) are as follows:

$$a_{1i} = \frac{e^i_{15}\mu^i_{11} - f^i_{15}g^i_{11}}{\mu^i_{11}\varepsilon^i_{11} - g^{i2}_{11}}, \quad b_{1i} = \frac{-\mu^i_{11}}{\mu^i_{11}\varepsilon^i_{11} - g^{i2}_{11}}, \quad c_{1i} = \frac{g^i_{11}}{\mu^i_{11}\varepsilon^i_{11} - g^{i2}_{11}}, \tag{A.1}$$

$$a_{2i} = \frac{f^i_{15}\varepsilon^i_{11} - e^i_{15}g^i_{11}}{\mu^i_{11}\varepsilon^i_{11} - g^{i2}_{11}}, \quad b_{2i} = \frac{g^i_{11}}{\mu^i_{11}\varepsilon^i_{11} - g^{i2}_{11}}, \quad c_{2i} = \frac{-\varepsilon^i_{11}}{\mu^i_{11}\varepsilon^i_{11} - g^{i2}_{11}}. \tag{A.2}$$

m_{1i}, m_{2i}, m_{3i} in Eq. (11) are as follows:

$$m_{1i} = c^i_{44} + \frac{\varepsilon^i_{11}f^{i2}_{15} - 2e^i_{15}f^i_{15}g^i_{11} + \mu^i_{11}e^{i2}_{15}}{\mu^i_{11}\varepsilon^i_{11} - g^{i2}_{11}}, \quad m_{2i} = \frac{f^i_{15}g^i_{11} - e^i_{15}\mu^i_{11}}{\mu^i_{11}\varepsilon^i_{11} - g^{i2}_{11}}, \tag{A.3}$$

$$m_{3i} = \frac{e^i_{15}g^i_{11} - f^i_{15}\varepsilon^i_{11}}{\mu^i_{11}\varepsilon^i_{11} - g^{i2}_{11}}. \tag{A.4}$$

Appendix B

The matrix $\mathbf{L}_n(p)$ in Eqs. (33) and (35) are as follows:

$$\mathbf{L}_n(p) = \mathrm{diag}\left[\,1/(\mathrm{e}^{2\lambda_{n1}h_1} - 1) \quad 1/(\mathrm{e}^{2\beta_n h_1} - 1) \quad 1/(\mathrm{e}^{2\beta_n h_1} - 1)\,\right]\mathbf{\Pi}_n(p), \tag{B.1}$$

where

$$\mathbf{\Pi}_n(p) = \begin{bmatrix} \frac{\lambda_{n2}}{\lambda_{n1}}(\mathrm{e}^{-2\lambda_{n2}h_2} - 1)M_{11} & \frac{\beta_n}{\lambda_{n1}}(\mathrm{e}^{-2\beta_n h_2} - 1)M_{12} & \frac{\beta_n}{\lambda_{n1}}(\mathrm{e}^{-2\beta_n h_2} - 1)M_{13} \\ \frac{\lambda_{n2}}{\beta_n}(\mathrm{e}^{-2\lambda_{n2}h_2} - 1)M_{21} & (\mathrm{e}^{-2\beta_n h_2} - 1)M_{22} & (\mathrm{e}^{-2\beta_n h_2} - 1)M_{23} \\ \frac{\lambda_{n2}}{\beta_n}(\mathrm{e}^{-2\lambda_{n2}h_2} - 1)M_{31} & (\mathrm{e}^{-2\beta_n h_2} - 1)M_{32} & (\mathrm{e}^{-2\beta_n h_2} - 1)M_{33} \end{bmatrix}, \tag{B.2}$$

$$\mathbf{M} = \mathbf{M}_1^{-1}\mathbf{M}_2. \tag{B.3}$$

Appendix C

The matrix $\mathbf{R}(\eta, \varsigma, p)$ in Eq. (69) is as follows

$$\mathbf{R}(\eta, \varsigma, p) = \frac{\cos\frac{\pi a}{d} - \cos\frac{\pi b}{d}}{\sin\frac{\pi u(\eta)}{d}} \sum_{n=1}^{\infty}\{2\widetilde{\mathbf{\Xi}}_n(\eta, \varsigma, p) - \mathbf{\Xi}\}\sin(\beta_n u(\eta))\cos(\beta_n x(\varsigma)), \quad -1 < \varsigma < 1, \tag{C.1}$$

where

$$\widetilde{\mathbf{\Xi}}_n = \begin{bmatrix} \alpha_{1n}c_{44} & \alpha_{2n}e_{15} & \alpha_{2n}f_{15} \\ \alpha_{2n}e_{15} & -\alpha_{2n}\varepsilon_{11} & -\alpha_{2n}g_{11} \\ \alpha_{2n}f_{15} & -\alpha_{2n}g_{11} & -\alpha_{2n}\mu_{11} \end{bmatrix}, \tag{C.2}$$

with

$$\alpha_{1n}(p) = \frac{(c_{44}g_{11}^2 - c_{44}\varepsilon_{11}\mu_{11} - e_{15}^2\mu_{11} - f_{15}^2\varepsilon_{11} + 2e_{15}f_{15}g_{11})\lambda_n}{c_{44}(g_{11}^2 - \varepsilon_{11}\mu_{11})\beta_n(\coth(\lambda_n h_1) + \coth(\lambda_n h_2))} + \frac{f_{15}^2\varepsilon_{11} + e_{15}^2\mu_{11} - 2e_{15}f_{15}g_{11}}{c_{44}(g_{11}^2 - \varepsilon_{11}\mu_{11})(\coth(\beta_n h_1) + \coth(\beta_n h_2))}, \tag{C.3}$$

$$\alpha_{2n} = \frac{1}{\coth(\beta_n h_1) + \coth(\beta_n h_2)}. \tag{C.4}$$

References

[1] Van Suchtelen J. Product properties: a new application of composite materials. Phillips Res Reports 1972;27:28–37.
[2] Harshe G, Dougherty JP, Newnham RE. Theoretical modeling of 3-0/0-3 magnetoelectric composites. Int J Appl Electromagn Mater 1993;4:161–71.
[3] Avellaneda M, Harshe G. Magnetoelectric effect in piezoelectric/magnetostrictive multiplayer (2-2) composites. J Intell Mater Syst Struct 1994;5:501–13.
[4] Nan CW. Magneto-electric effect in composites of piezoelectric and piezomagnetic phases. Phys Rev 1994;B B50:6082–8.
[5] Benveniste Y. Magneto-electric effect in fibrous composites with piezoelectric and piezomagnetic phases. Phys Rev 1995;B B51:16424–7.
[6] Li JY, Dunn ML. Micromechanics of magneto-electro-elastic composite materials: average fields and effective behavior. J Intell Mater Syst Struct 1998;9:404–16.
[7] Pan E. Exact solution for simply supported and multilayered magneto-electro-elastic plates. ASME J Appl Mech 2001;68:608–18.
[8] Wang X, Shen YP. Inclusions of arbitrary shape in magnetoelectroelastic composite materials. Int J Engng Sci 2003;41:85–102.
[9] Lage RG, Soares CMM, Soares CAM, Reddy JN. Layerwise partial mixed finite element analysis of magneto-electro-elastic plates. Compos Struct 2004;82:1293–301.
[10] Sih GC, Song ZF. Magnetic and electric poling effects associated with crack growth in $BaTiO_3$–$CoFe_2O_4$ composite. Theor Appl Fract Mech 2003;39:209–27.
[11] Gao CF, Hannes K, Herbert B. Crack problems in magnetoelectroelastic solids. Part I: exact solution of a crack. Int J Engng Sci 2003;41:969–81.
[12] Gao CF, Tong P, Zhang TY. Fracture mechanics for a mode III crack in a magnetoelectroelastic solid. Int J Solids Struct 2004;41:6613–29.
[13] Zhou ZG, Wang B, Sun YG. Two collinear interface cracks in magneto-electro-elastic composites. Int J Engng Sci 2004;42:1155–67.
[14] Hu KQ, Li GQ, Zhong Z. Fracture of a rectangular piezoelectromagnetic body. Mech Res Commun 2006;33:482–92.
[15] Du JK, Shen YP, Ye DY, Yue FR. Scattering of anti-plane shear waves by a partially debonded magneto-electro-elastic circular cylindrical inhomogeneity. Int J Engng Sci 2004;42:887–913.
[16] Feng WJ, Su RKL, Liu YQ. Scattering of SH waves by an arc-shaped interface crack between a cylindrical magneto-electro-elastic inclusion and matrix with the symmetry of 6 mm. Acta Mech 2006;183:81–102.
[17] Hou PF, Leung AYT. The transient responses of magneto-electro-elastic hollow cylinders. Smart Mater Struct 2004;13:762–76.
[18] Zhou ZG, Wu LZ, Wang B. The dynamic behavior of two collinear interface cracks in magneto-electro-elastic materials. Eur J Mech A/Solids 2005;24:253–62.
[19] Feng WJ, Xue Y, Zou ZZ. Crack growth of an interface crack between two dissimilar magneto-electro-elastic materials under anti-plane mechanical and in-plane electric magnetic impact. Theor Appl Fract Mech 2005;43:376–94.
[20] Hu KQ, Li GQ. Constant moving crack in a magnetoelectroelastic material under anti-plane shearing loading. Int J Solids Struct 2005;42:2823–35.
[21] Hu KQ, Kang YL, Li GQ. Moving crack at the interface between two dissimilar magnetoelectroelastic materials. Acta Mech 2006;182:1–16.
[22] Feng WJ, Su RKL. Dynamic internal crack problem of a functionally graded magneto-electro-elastic strip. Int J Solids Struct 2006;43:5196–216.
[23] Kwon SM, Son MS, Lee KY. Transient behavior in a cracked piezoelectric layered composites: anti-plane problem. Mech Mater 2002;34:593–603.
[24] Zhang TY, Zhao MH, Tong P. Fracture of piezoelectric ceramics. Adv Appl Mech 2002;38:147–289.
[25] Erdogan F, Gupta GD. On the numerical solution of singular integral equations. Q Appl Math 1972;29:525–39.
[26] Li XF, Lee KY. Electroelastic behavior of a rectangular piezoelectric ceramic with an antiplane shear crack at arbitrary position. Eur J Mech A/Solids 2004;23:645–58.
[27] Pak YE. Crack extension force in a piezoelectric material. J Appl Mech 1990;57:647–53.
[28] Soh AK, Fang DN, Lee KL. Analysis of a bi-piezoelectric ceramic layer with an interfacial crack subjected to anti-plane shear and in-plane electric loading. Eur J Mech A/Solids 2000;19:961–77.
[29] Wang XY, Yu SW. Transient response of a crack in a piezoelectric strip objected to the mechanical and electrical impacts: mode III problem. Int J Solids Struct 2000;37:5795–808.